11-7-2017

# Macroscopic Anisotropic Bone Material Properties in Children with Severe *Osteogenesis imperfecta*

Carolyne Albert
*Marquette University*, carolyne.albert@marquette.edu

John Jameson
*Marquette University*, john.jameson@marquette.edu

Sergey Tarima
*Medical College of Wisconsin*

Peter Smith
*Rush University Medical Center*

Gerald Harris
*Marquette University*, gerald.harris@marquette.edu

Accepted version. *Journal of Biomechanics,* Vol. 64, (November 7, 2017): 103-111. DOI. 

*Journal of Biomechanics*, Vol. 64, (November, 2017):103-111. DOI. 

## Contents

# Macroscopic anisotropic bone material properties in children with severe *osteogenesis imperfecta*

Carolyne Albert
Orthopaedic and Rehabilitation Engineering Center (OREC),
Department of Biomedical Engineering, Marquette University, Milwaukee, WI
John Jameson
Orthopaedic and Rehabilitation Engineering Center (OREC),
Department of Biomedical Engineering, Marquette University, Milwaukee, WI
Sergey Tarima
Division of Biostatistics, Medical College of Wisconsin, Milwaukee, WI
Peter Smith
Shriners Hospitals for Children, Chicago, IL
Department of Orthopedic Surgery, Rush University Medical Center, Chicago, IL
Gerald Harris
Orthopaedic and Rehabilitation Engineering Center (OREC),
Department of Biomedical Engineering, Marquette University, Milwaukee, WI
Shriners Hospitals for Children, Chicago, IL

## Abstract

Children with severe *osteogenesis imperfecta* (OI) typically experience numerous fractures and progressive skeletal deformities over their lifetime. Recent studies proposed finite element models to assess fracture risk and guide clinicians in determining appropriate intervention in children with OI, but lack of appropriate material property inputs remains a challenge. This study aimed to characterize macroscopic anisotropic cortical bone material properties and investigate relationships with bone density measures in children with severe OI. Specimens were obtained from tibial or femoral shafts of nine children with severe OI and five controls. The specimens were cut into beams, characterized in bending, and imaged by synchrotron radiation X-ray micro-computed tomography. Longitudinal modulus of elasticity, yield strength, and bending strength were 32–65% lower in the OI group ($p < 0.001$). Yield strain did not differ between groups ($p \geq 0.197$). In both groups, modulus and strength were lower in the transverse direction ($p \leq 0.009$), but anisotropy was less pronounced in the OI group. Intracortical vascular porosity was almost six times higher in the OI group ($p < 0.001$), but no differences

were observed in osteocyte lacunar porosity between the groups ($p = 0.086$). Volumetric bone mineral density was lower in the OI group ($p < 0.001$), but volumetric tissue mineral density was not ($p = 0.770$). Longitudinal OI bone modulus and strength were correlated with volumetric bone mineral density ($p \leq 0.024$) but not volumetric tissue mineral density ($p \geq 0.099$). Results indicate that cortical bone in children with severe OI yields at the same strain as normal bone, and that their decreased bone material strength is associated with reduced volumetric bone mineral density. These results will enable the advancement of fracture risk assessment capability in children with severe OI.

## Keywords

Osteogenesis imperfecta; Pediatric bone; Material properties; Synchrotron radiation micro-computed tomography; Fracture risk

## 1. Introduction

Osteogenesis imperfecta (OI) is a genetic bone fragility disorder affecting between 1/20,000 and 1/5000 births (Byers and Steiner, 1992, Marini, 2011). There is no cure, and individuals are affected throughout their lifetime. OI type III, the most severe phenotype in individuals surviving birth, typically results in numerous bone fractures and progressive skeletal deformities, such as pronounced bowing of long bones (Sillence et al., 1979). Clinical management usually involves antiresorptive drugs and physical rehabilitation. Corrective surgery is sometimes used to straighten a bowed tibia or femur with the aim to improve mobility and prevent fracture. However, there is no quantitative method by which to assess fracture risk or the potential benefit of surgical or rehabilitative interventions in children with OI. Recent studies proposed using finite element models to quantify tibial and femoral fracture risk in children with OI (Fritz et al., 2009a, Fritz et al., 2009b, Caouette et al., 2014, Caouette et al., 2016). These models could prove useful to clinicians in determining safe activity levels or when to perform corrective surgery. However, a major challenge to these fracture risk assessment efforts remains the paucity of macroscopic-scale material property data in children with severe OI.

Macroscopic bone material properties have been studied in small groups of children with OI (Albert Albert et al., 2013, Albert et al., 2014, Vardakastani et al., 2014, Imbert et al., 2015). Bone material strength and modulus of elasticity were confirmed to be reduced in these children compared to controls (Imbert et al., 2015). Abnormally elevated intracortical vascular porosity was also observed in children with OI (Jameson Jameson et al., 2013, Pazzaglia et al., 2013, Albert et al., 2013, Albert et al., 2014, Imbert et al., 2015), and was found to have a negative effect on cortical bone modulus and strength (Albert et al., 2014, Vardakastani et al., 2014, Imbert et al., 2015). These studies, however, were not focused specifically on children with severe OI, who tend to experience the most fractures, and only one study (Albert et al., 2014) examined anisotropy (i.e., directional dependence) of the bone material properties.

The objectives of the current study were to: (1) characterize the anisotropic material properties of cortical bone in children with severe OI at the macroscopic scale; (2) compare these properties to those of pediatric controls; and (3) investigate relationships between material properties and measures of bone material density in this patient population. The results of this study will enable improved fracture risk assessment capabilities in children with severe OI.

# 2. Materials and methods

## 2.1. Bone specimens

Nine cortical osteotomy specimens were collected from the tibial or femoral diaphyses of seven children and adolescents (age 1–16 years) with severe OI (OI group), Table 1. Six of these children were diagnosed with OI type III. The seventh (donor 7) has a less common recessive form, OI type VIII, with clinical severity similar to that of OI type III. These specimens were obtained during routine surgical procedures at Shriners Hospitals for Children – Chicago under informed consent/assent and an approved IRB protocol (Western IRB WIRB#20160453, Marquette University #HR-2167). The specimens were fresh-frozen and stored below −20 °C prior to testing.

Table 1. Specimen description and donor details. For each specimen, the numbers of machined beams tested of each orientation relative to the long bone axis, *i.e.*, longitudinal (*L*) or transverse (*T*), is indicated. Of those beams, a subset (*numbers in parentheses*) was imaged by SRμCT following mechanical testing.

| **Donor** | **Gene affected** | **Specimen** | **Age (years)** | **Gender** | **Harvest site** | **Surgery notes** | **Beams tested (*Beams imaged*)** | |
|---|---|---|---|---|---|---|---|---|
| | | | | | | | ***L*** | ***T*** |
| *OI group* | | | | | | | | |
| 1 | *COL1A1* | OI 1 | 1 | M | Tibia | Deformity correction | 2 (0) | 0 (0) |
| 2 | *COL1A2* | OI 2[a] | 3 | F | Femur | Deformity correction | 2 (1) | 2 (1) |
| | | OI 3[a] | | | Femur | Deformity correction | 4 (1) | 2 (1) |
| 3 | Not available | OI 4 | 9 | F | Tibia | Rod revision | 1 (1) | 1 (1) |
| 4 | Not available | OI 5 | 11 | M | Femur[c] | Fracture two weeks prior | 4 (2) | 1 (1) |
| 5 | *COL1A1* | OI 6 | 13 | F | Tibia | Deformity correction | 2 (2) | 1 (1) |
| 6 | *COL1A1* | OI 7[b] | 13 | M | Femur | Rod revision | 4 (0) | 3 (0) |
| | | OI 8[b] | 14 | | Tibia | Rod revision | 2 (2) | 0 (0) |
| 7 | *LEPRE1* | OI 9 | 16 | M | Tibia | Deformity correction | 6 (2) | 3 (2) |

| Donor | Gene affected | Specimen | Age (years) | Gender | Harvest site | Surgery notes | Beams tested (*Beams imaged*) | |
|---|---|---|---|---|---|---|---|---|
| | | | | | | | ***L*** | ***T*** |
| *Control group* | | | | | | | | |
| 8 | Normal | C 1 | 8 | M | Femur | n/a | 6 (2) | 6 (2) |
| 9 | Normal | C 2 | 10 | F | Femur | n/a | 6 (2) | 6 (2) |
| 10 | Normal | C 3 | 10 | F | Tibia | n/a | 6 (2) | 6 (2) |
| 11 | Normal | C 4 | 11 | F | Tibia | n/a | 6 (2) | 6 (2) |
| 12 | Normal | C 5 | 11 | M | Femur | n/a | 6 (2) | 6 (2) |

*a Specimens OI 2 and OI 3 were obtained from contralateral femurs of the same donor (donor 2) during a bilateral corrective procedure.*
*b Specimens OI 7 and OI 8 were obtained from a single donor (donor 6) during surgical procedures that took place eight months apart.*
*c All specimens were obtained from the long bone mid-diaphysis, with the exception of specimen OI 5, which was obtained from the proximal region of the femur diaphysis.*

For comparison, cortical bone specimens were obtained from the femoral and tibial diaphyses of five deceased donors (control group, age 8–11 years, cause of death unknown).

## 2.2. Specimen preparation

Each specimen was cut into 2–12 rectangular beams (Table 1) using a precision sectioning saw (IsoMet™ Low Speed Saw, Buehler®, Lake Bluff, IL, USA) and a 0.3 mm-thick diamond blade (IsoMet 15HC Model 11-4244, Buehler®, Lake Bluff, IL, USA). The beams were 5–6 mm long, with the long beam axis being either parallel to the long diaphyseal axis (longitudinal beams) or in the circumferential direction of the outer cortex (transverse beams) (Albert et al., 2013). Beam depth (0.633 mm ± 0.042 mm) and base (1.021 mm ± 0.039 mm) were measured with a digital micrometer (Model 293-340, Mitutoyo Corporation, Japan).

## 2.3. Mechanical testing

The beams were tested in three-point bending on a custom-designed jig using methodology validated for small bone specimens (Albert et al., 2013). A span length of 4.0 mm was chosen to accommodate the small osteotomy specimens collected for this study. Mechanical testing was performed on an electromechanical testing machine (Model 3345, Instron®, Norwood, MA, USA) with a 50 N load cell (Model 2519-102, Instron®, Norwood, MA, USA). The test was controlled using Bluehill 2 Software (Instron®, Norwood, MA, USA). Beam deflection at mid-span was determined as the vertical displacement of the loading nose relative to the supports, measured with a linear variable differential transformer (Model 2601-092, Instron®, Norwood, MA, USA). Five cycles of pre-conditioning (0.05–0.5 N) were applied at a crosshead displacement rate of 0.2 mm/min, followed by a ramp to failure at a constant beam deflection rate of 2.0 mm/min. The beams were kept hydrated during the test using a

drop of buffered saline, which remained in place on the tensile surface of the beam by surface tension for the duration of the test (less than 2 min). Load, crosshead displacement, and beam deflection were sampled at 100 Hz. Mid-span stress and strain at the tensile surface of the beam were calculated from the load and deflection data (ASTM-D790-07, 2006; Albert Albert et al., 2013, Albert et al., 2014). The following material properties were calculated from the stress-strain data obtained during the ramp to failure using Matlab (R2012a, Mathworks, Natick, MA, USA), correcting for shear effects (see Supplement - Shear Effects Correction): bending strength, yield strength, modulus of elasticity, and yield strain.

## 2.4. Synchrotron radiation X-ray micro-computed tomographic imaging (SRμCT)

After mechanical testing, cortical bone density and porosity measures were obtained for a subset of beams (Table 1) using SRμCT (Beamline 8.3.2, Advanced Light Source, Lawrence Berkeley National Laboratory, Berkeley, CA, USA). These methods were described in detail in earlier works (Jameson et al., 2013; Albert et al., 2014). In short, each scan consisted of 1025 radiographs collected at a monochromatic beam energy of 17 keV over a continuous 180° rotation using a pco.edge sCMOS camera (PCO-TECH Inc., Romulus, MI, USA). The camera was mounted to a high resolution X-ray microscope (Optique Peter, Lentilly, France) containing a 10× objective lens (Mitutoyo Corporation, Kawasaki, Japan) and a 50 μm thick lutetium aluminum garnet ($Lu_3Al_5O_{12}$) scintillator to convert X-rays into visible light. This configuration resulted in a 1.7 mm × 1.4 mm field of view, with an isotropic imaged pixel size of 0.65 μm. Tomographic reconstruction of each scan was performed with Octopus 8.6 software (inCT, Ghent, Belgium), resulting in a 32-bit grayscale dataset with 2160 slices each having 2560 × 2560 pixels.

Visual inspection of these scans revealed the presence of a small region of microdamage resulting from mechanical testing, extending approximately 0.25 mm on either side of the test-induced fracture (Fig. 1). Imaging measurements were obtained within a 0.6 $mm^3$ rectangular prismatic region of interest located at least 0.5 mm away from the fracture site to exclude the region in which test-induced microdamage was present (Fig. 1).

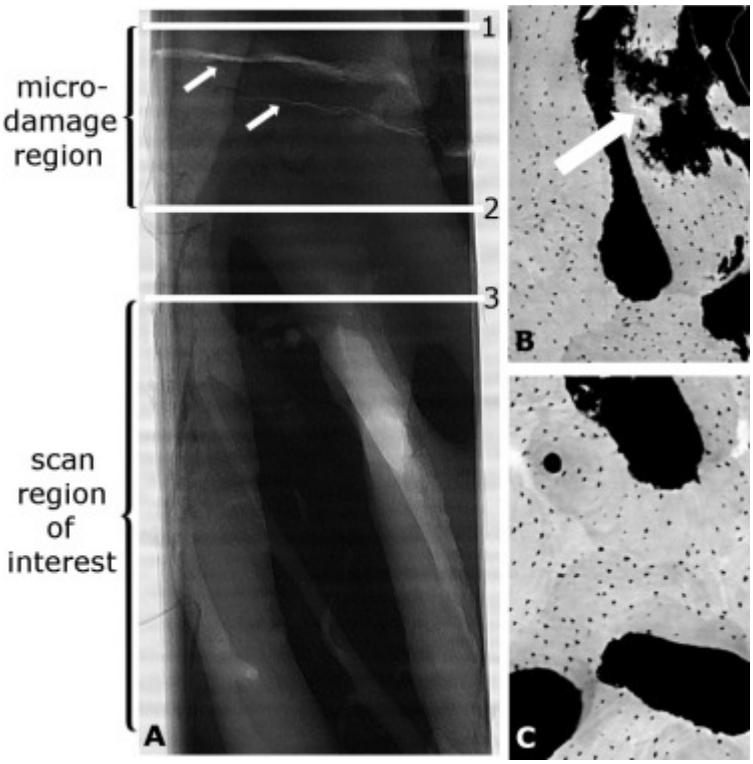


Fig. 1. Scan of representative beam in the OI group (specimen OI 5). (A) Longitudinal radiographic view of a beam obtained from specimen OI 5, where the test-induced fracture can be seen (see small white arrows) and the region containing microdamage extends approximately 0.25 mm on either side of the fracture, *i.e.*, between lines 1 and 2. (B) Reconstructed image of a cross-section adjacent to the test-induced fracture, where microdamage can be seen (see bold white arrow). (C) Cross-section obtained within the region of interest, approximately 0.5 mm away from the middle of the test-induced fracture (i.e., below line 3), where no microdamage was visible.

The total porosity in each beam was calculated as the sum of the contributions from both vascular and osteocyte lacunar porosities. In accordance with the established nomenclature (Parfitt et al., 1987, Cooper et al., 2003), the vascular porosity was defined as the canal volume per tissue volume (*Ca.V*/*TV*) and included Haversian canals, Volkmann canals, and resorption spaces (Cardoso et al., 2013). The osteocyte lacunar porosity was defined as the lacunar total volume per tissue volume (*Lc.TV*/*TV*). These porosity contributions were determined using Fiji software (Schneider et al., 2012), a distribution of ImageJ v1.49f (National Institutes of Health, Bethesda, MD, USA) and the plug-in BoneJ (Doube et al., 2010). Pores having a volume <82 $\mu m^3$ were considered as noise and removed, while pores with a volume >2000 $\mu m^3$ were assumed to be part of the vascular porosity. These limits were based on previous laser scanning confocal microscopy and SRμCT studies in human bone (McCreadie et al., 2004, Carter et al., 2013, Dong et al., 2014). Due to the monochromatic X-ray source, bone density measures were calculated for each beam from: (1) the 32-bit gray values, which corresponded directly to the linear attenuation coefficients; and (2) the X-ray mass attenuation coefficient of bone, $(\mu/\rho)_{bone}$, which is a material constant that depends on X-ray beam energy. According to reference tables provided by the National Institute of Standards and Technology, $(\mu/\rho)_{bone}$ is equal to 6.41 $cm^2/g$ at 17 keV (Hubbell 1982).

Volumetric bone mineral density, *vBMD*, was determined by dividing the mean linear attenuation coefficient of the total volume within the beam (*i.e.*, including both bone and porosity voxels) in the scanned region of interest by $(\mu/\rho)_{bone}$. Volumetric tissue mineral density, *vTMD*, was evaluated by

segmenting out all non-bone voxels from the original volume using a histogram-based threshold (Ridler and Calvard, 1978), calculating the mean linear attenuation coefficient of the remaining bone voxels, and dividing this number by $(\mu/\rho)_{bone}$. The X-ray beam energy was calibrated prior to imaging using silver and germanium foils, which have known peaks in X-ray absorption at 25.514 keV and 11.103 keV, respectively. The energy resolution of the beam varies by less than 1% (MacDowell et al., 2012). Three-dimensional visualizations of the imaging datasets were performed using the Volume Rendering module in Avizo 9.2.0 software (FEI, Hillsboro, OR, USA).

### 2.5. Statistical analysis

Statistical analysis employed linear mixed models with specimen number as a random factor and likelihood ratio tests for investigating statistical significance. The random effect of specimen number was one-dimensional Gaussian for analyses of mechanical properties (longitudinal and transverse properties were analyzed separately) and two-dimensional Gaussian for analyses of imaging measures (analyses of imaging parameters combined beams of both orientations). P-values smaller than 0.05 were considered statistically significant. Linear mixed model analyses were performed to compare the material properties and imaging measures between the groups of specimens (OI vs. control group), and the material properties between different beam orientations (longitudinal vs. transverse) within each group. Similarly, linear mixed models were used to explore associations between mechanical properties (dependent variables) and the imaging measures (independent variable) in children with OI, controlling for possible clustering within specimen by including a specimen random effect.

## 3. Results

### 3.1. Material properties

Average material properties for each specimen are presented in Table 2. Properties are compared between the two groups (OI vs. control) and between beam orientations (longitudinal vs. transverse) in Table 3.

Table 2. Longitudinal (*L*) and transverse (*T*) material properties of cortical bone in children with severe OI (OI group) and pediatric controls (control group). Mean (standard deviation) for each specimen.

| **Spec.** | **Age** | **Site** | **Modulus of elasticity (GPa)** | | **Yield strength (MPa)** | | **Yield strain (%)** | | **Bending strength (MPa)** | |
|---|---|---|---|---|---|---|---|---|---|---|
| *OI group* | | | *L* | *T* | *L* | *T* | *L* | *T* | *L* | *T* |
| OI 1 | 1 | Femur | 7.8 | – | 81 | – | 1.0 | – | 122 | – |
| OI 2 | 3 | Femur | 7.2 | 2.2 | 71 | 19 | 1.0 | 0.9 | 98 | 21 |
| OI 3 | 3 | Femur | 6.0 (0.4) | 1.9 | 66 (7) | 16 | 1.1 (0.1) | 0.9 | 94 (7) | 24 |
| OI 4 | 9 | Tibia | 3.2 | 2.1 | 40 | 13 | 1.3 | 0.6 | 80 | 15 |

| Spec. | Age | Site | Modulus of elasticity (GPa) | | Yield strength (MPa) | | Yield strain (%) | | Bending strength (MPa) | |
|---|---|---|---|---|---|---|---|---|---|---|
| OI 5 | 11 | Femur | 5.7 (1.8) | 3.7 | 72 (20) | 37 | 1.3 (0.2) | 1.0 | 98 (26) | 54 |
| OI 6 | 13 | Tibia | 4.4 | 3.1 | 51 | 32 | 1.1 | 1.0 | 79 | 42 |
| OI 7 | 13 | Femur | 6.8 (1.0) | 6.3 (1.8) | 75 (18) | 61 (22) | 1.1 (0.1) | 1.0 (0.2) | 113 (29) | 87 (38) |
| OI 8 | 14 | Tibia | 2.5 | – | 33 | – | 1.3 | – | 46 | – |
| OI 9 | 16 | Tibia | 5.8 (1.5) | 3.8 (1.0) | 52 (15) | 37 (17) | 0.9 (0.1) | 1.0 (0.3) | 72 (25) | 47 (17) |
| *Control group* | | | | | | | | | | |
| C 1 | 8 | Femur | 13.3 (1.1) | 4.7 (1.4) | 152 (13) | 44 (12) | 1.1 (0.1) | 1.0 (0.1) | 236 (23) | 63 (13) |
| C 2 | 10 | Femur | 12.0 (0.7) | 6.3 (1.2) | 132 (12) | 61 (8) | 1.1 (0.1) | 1.0 (0.1) | 208 (22) | 98 (4) |
| C 3 | 10 | Tibia | 12.8 (1.4) | 6.4 (0.7) | 151 (11) | 73 (13) | 1.2 (0.1) | 1.1 (0.1) | 252 (15) | 109 (23) |
| C 4 | 11 | Tibia | 14.3 (1.3) | 3.5 (1.0) | 159 (14) | 34 (13) | 1.1 (0.1) | 0.9 (0.1) | 270 (35) | 59 (23) |
| C 5 | 11 | Femur | 13.7 (1.9) | 4.2 (2.1) | 151 (15) | 40 (21) | 1.1 (0.1) | 0.9 (0.1) | 255 (44) | 67 (30) |

Note: standard deviation is presented when a minimum of three beams were tested for the specimen.

Table 3. Comparison of cortical bone material properties between children with severe OI (OI group) and pediatric controls (control group) tested in the longitudinal vs. transverse directions. Mean (standard error). P-values based on linear mixed models. Elastic modulus and strength were lower in children with OI vs. controls.

| Material property | OI group | Control group | P-value (OI vs. control) |
|---|---|---|---|
| *Modulus of elasticity* (*GPa*) | | | |
| Longitudinal | 5.4 (0.5) | 13.2 (0.7) | **<0.001** |
| Transverse | 3.4 (0.6) | 5.0 (0.6) | 0.061 |
| P-value (longitudinal vs. transverse) | **<0.001** | **<0.001** | |

| **Material property** | **OI group** | **Control group** | **P-value (OI vs. control)** |
|---|---|---|---|
| *Yield strength* (*MPa*) | | | |
| Longitudinal | 59 (5) | 149 (7) | **<0.001** |
| Transverse | 31 (7) | 51 (7) | 0.055 |
| P-value (longitudinal vs. transverse) | **<0.001** | **<0.001** | |
| *Yield strain* (*%*) | | | |
| Longitudinal | 1.1 (0.0) | 1.1 (0.1) | 0.893 |
| Transverse | 0.9 (0.0) | 1.0 (0.0) | 0.197 |
| P-value (longitudinal vs. transverse) | **0.009** | **<0.001** | |
| *Bending strength* (*MPa*) | | | |
| Longitudinal | 86 (9) | 244 (11) | **<0.001** |
| Transverse | 42 (10) | 79 (10) | **0.015** |
| P-value (longitudinal vs. transverse) | **<0.001** | **<0.001** | |

P-values in bold font emphasize the comparisons that are statistically significant (P-values <0.05).

In both groups, the properties exhibited anisotropy (Table 3). Modulus of elasticity, yield strength, yield strain, and bending strength were lower in the transverse vs. longitudinal directions ($p \leq 0.009$). The effect of beam orientation (*i.e.*, anisotropy) on these properties, however, was less pronounced in the OI group. For example, the average ratio of longitudinal to transverse modulus, calculated as the average of the ratios obtained per specimen, was 2.6 for the control group but only 1.6 for the OI group. Similarly, the average ratio of longitudinal/transverse yield strength was 2.9 in the control group but only 1.9 in the OI group.

Between the two groups of donors, longitudinal modulus, yield strength, and bending strength, were significantly lower in the OI group, as was transverse bending strength ($p \leq 0.015$, Table 3). Theses properties were on average 47–65% lower in the OI group *vs.* controls. Transverse modulus and yield strength were also lower in the OI group, although these differences were not statistically significant ($p \geq 0.055$). No significant difference in yield strains were observed between the groups ($p \geq 0.197$).

## 3.2. Bone density

Visualization of the beam specimens indicated a high degree of variability in cortical bone structure within the OI group, with some beams displaying numerous small intracortical pores and others showing large pores that occupied over 50% of the beam volume. SRμCT scans from representative longitudinal beams within each group are illustrated in Fig. 2.

Video 1.

https://ars.els-cdn.com/content/image/1-s2.0-S0021929017304591-mmc2.mp4

Video 2.

https://ars.els-cdn.com/content/image/1-s2.0-S0021929017304591-mmc3.mp4

Video 3.

https://ars.els-cdn.com/content/image/1-s2.0-S0021929017304591-mmc4.mp4

Video 4.

https://ars.els-cdn.com/content/image/1-s2.0-S0021929017304591-mmc5.mp4

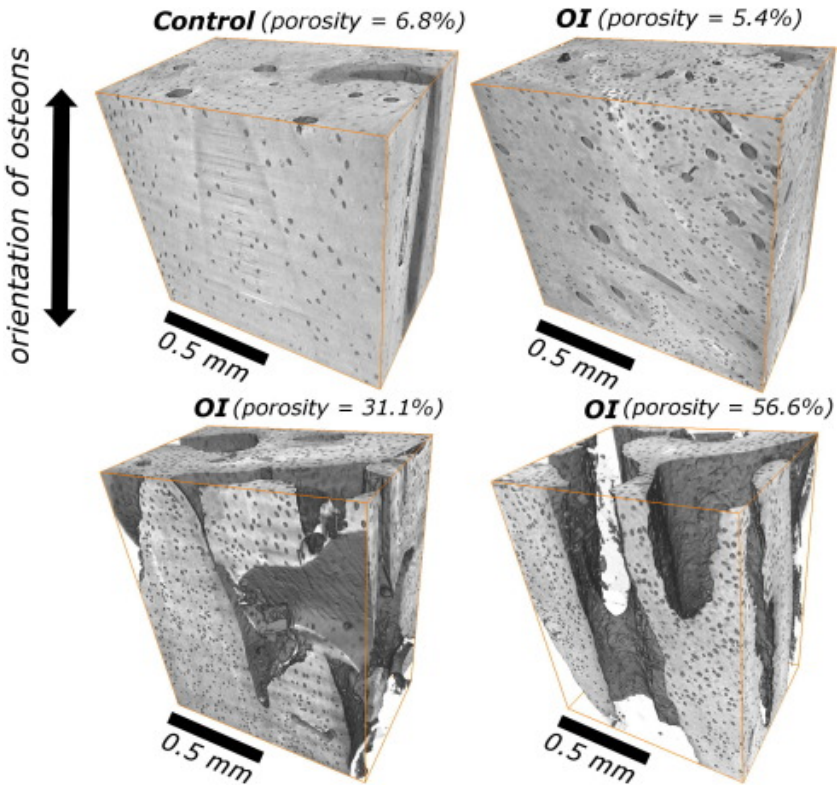


Fig. 2. Synchrotron radiation X-ray micro-computed tomographic scans of cortical bone structure from longitudinal beam specimens. Top Left: femur specimen from an 11 year-old male control donor (specimen *C 5;* bone volume fraction $V_f$ = *0.94*). Top Right: tibia specimen from a 13 year-old female with severe OI and high $V_f$ (specimen *OI 6*; $V_f$ = 0.96). Lower Left: femur specimen from 3 year-old female with severe OI and intermediate $V_f$ (specimen *OI 3*; $V_f$ = 0.71). Lower Right: femur specimen from an 11 year-old male with severe OI and low $V_f$ (specimen *OI 5*; $V_f$ = 0.44). Double-sided arrows indicate the orientation of the osteons. Scale bars represent 0.5 mm. See Video 1, Video 2, Video 3, Video 4 for 3 D visualization of each of these scans.

On average, vBMD was 22% lower in the OI group *vs.* controls ($p \leq 0.001$), Table 4. The vTMD, on the other hand, did not differ between the groups ($p = 0.770$). Average total porosity was 29.81% in the OI group, compared to 6.18% for the controls ($p < 0.001$). Average vascular porosity was nearly six times higher in the OI *vs*. control group, *i.e.*, 28.76% *vs*. 5.03%, respectively ($p < 0.001$). Lacunar porosity, however, did not differ significantly between the groups ($p = 0.086$).

Table 4. Cortical bone density and porosity measures for each group. Total porosity is decomposed in to vascular (Ca.V/TV) and osteocyte lacunar (Lc.TV/TV) contributions. Means (standard errors) and p-values based on linear mixed models with specimen random effect.

| Imaging parameter | OI group | Control group | P-value (OI vs. control) |
|---|---|---|---|
| *vBMD* (gHA/cm$^3$) | 0.77 (0.04) | 0.99 (0.04) | <0.001 |
| *vTMD* (gHA/cm$^3$) | 1.05 (0.02) | 1.04 (0.02) | 0.770 |
| *Total porosity* (*%*) | 29.81 (3.49) | 6.18 (3.90) | <0.001 |
| *Ca.V*/*TV* (%) | 28.76 (3.45) | 5.03 (3.88) | <0.001 |
| *Lc.TV*/*TV* (%) | 1.51 (0.10) | 1.24 (0.11) | 0.086 |

## 3.3. Relationships between bone material properties and imaging measures in OI

Relationships between longitudinal bone material properties and the imaging measures are presented in Table 5 and Fig. 3. Longitudinal modulus of elasticity and both strength measures were correlated positively with vBMD ($p \leq 0.024$) but no significant association was observed between material properties and vTMD. Modulus of elasticity and strength tended to decrease with increasing total porosity, but the relationships were not found to be statistically significant ($p \geq 0.062$). Finally, yield strain was not significantly correlated with any imaging parameter.

Table 5. Relationships between longitudinal mechanical properties and bone imaging measures (volumetric bone mineral density *vBMD*, volumetric tissue mineral density *vTMD*, and total intracortical porosity) in children with severe OI based on simple linear regression analysis. Modulus of elasticity and strength were positively correlated with *vBMD* but not with *vTMD*. Adjusted $R^2$ were obtained from a simple linear regression model.

| Mechanical property | Density measure (predictor) | Intercept (SE) | Slope (SE) | P-value for the slope | Adjusted $R^2$ |
|---|---|---|---|---|---|
| Modulus of elasticity (GPa) | vBMD (gHA/cm$^3$) | 0.01 (1.76) | 6.70 (2.37) | **0.010** | 0.30 |
| | vTMD (gHA/cm$^3$) | −3.66 (6.42) | 8.19 (6.17) | 0.159 | 0.06 |
| | Total porosity (%) | 6.94 (1.03) | −0.07 (0.03) | 0.062 | 0.22 |
| Yield strength (MPa) | vBMD (gHA/cm$^3$) | 2.97 (18.53) | 70.05 (24.53) | **0.014** | 0.19 |
| | vTMD (gHA/cm$^3$) | −50.43 (63.79) | 100.46 (61.20) | 0.099 | 0.12 |
| | Total porosity (%) | 77.46 (10.68) | −0.74 (0.27) | 0.149 | 0.10 |
| Yield strain (%) | vBMD (gHA/cm$^3$) | 1.26 (0.20) | −0.16 (0.26) | 0.519 | 0.04 |
| | vTMD (gHA/cm$^3$) | 2.06 (0.67) | −0.88 (0.64) | 0.196 | −0.08[a] |
| | Total porosity (%) | 1.10 (0.12) | 0.00 (0.00) | 0.19 | 0.07 |

| Mechanical property | Density measure (predictor) | Intercept (SE) | Slope (SE) | P-value for the slope | Adjusted $R^2$ |
|---|---|---|---|---|---|
| | vBMD (gHA/cm$^3$) | 11.06 (27.15) | 92.71 (36.38) | **0.024** | 0.20 |
| Bending strength (MPa) | vTMD (gHA/cm$^3$) | −3.09 (94.96) | 77.46 (91.11) | 0.366 | −0.02[a] |
| | Total porosity (%) | 115.32 (13.75) | −1.13 (0.35) | 0.062 | 0.22 |

*P-values in bold font emphasize the comparisons that are statistically significant (P-values <0.05).*

*a Note that negative $R^2$ indicates that the model contains some non-significant terms that do not improve the prediction properties.*

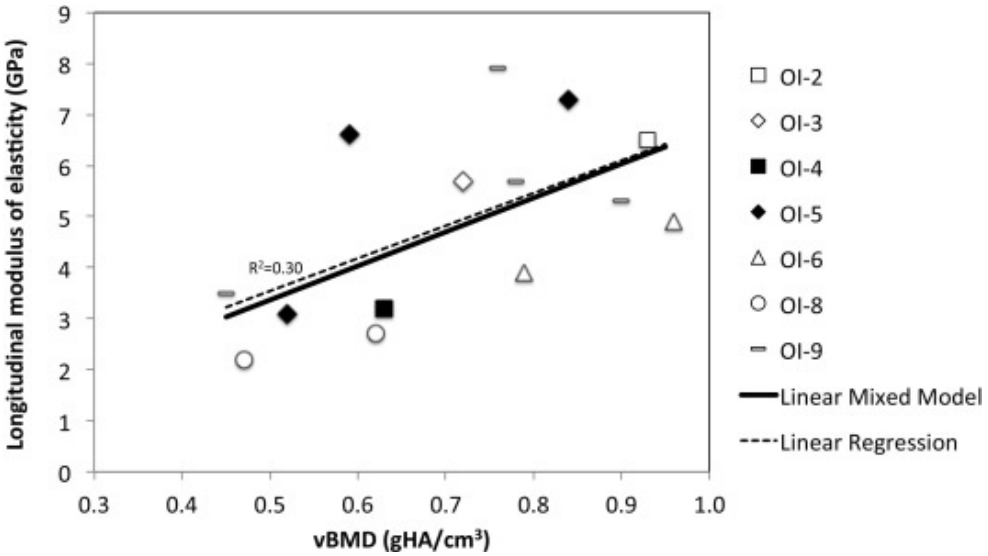


Fig. 3. Relationship between longitudinal modulus of elasticity and volumetric bone volume fraction in the OI group. A simple linear regression with $R^2$ is superposed to the linear mixed model.

## 4. Discussion

Children with severe OI typically experience multiple fractures over their lifetime. Recent research has been aimed at enabling fracture risk assessment in these children by finite element modeling (Fritz et al., 2009a, Fritz et al., 2009b, Caouette et al., 2014, Caouette et al., 2016), with the goal of developing and improving preventive treatments to reduce fracture occurrences. However, lack of appropriate macroscopic-scale anisotropic material property inputs for these models remains a major challenge to these efforts. This study characterized the anisotropic macroscopic material properties of cortical bone from tibial and femoral diaphyses of children with severe OI, compared these properties to those of controls, and explored relationships between OI bone material properties and bone material density measures.

Bending tests are used commonly for bone material characterization. When testing small bone specimens in bending, special attention should be given to beam dimensions. Modulus of elasticity of

bone measured in bending tends to be lower when beam depth is smaller than 500 µm (Choi et al., 1990), therefore a beam depth of approximately 600 µm was selected for this study. A minimum span/beam depth ratio of 16 or 20 is sometimes recommended to avoid error resulting from shear effects (ASTM-D790-07, 2006, Wallace et al., 2014). In this study, a span of 4 mm was chosen to accommodate the small osteotomy specimens available, providing a span/depth ratio of approximately seven; hence the effect of shear deformation was accounted for when calculating the material properties.

Bone density measures (Table 4) and longitudinal material properties (Table 2, Table 3) for the control group were similar to values reported previously for pediatric cortical bone (Hirsch and Evans, 1965, Currey and Butler, 1975, Currey and Pond, 1989, Ohman et al., 2011, Jameson et al., 2013, Imbert et al., 2015). Results in the OI group (Table 2, Table 3, Table 4) were also comparable to values reported in earlier studies of cortical bone in children with mild to severe OI (Albert et al., 2014, Vardakastani et al., 2014, Imbert et al., 2015). In contrast to these earlier OI studies, the current study is focused more specifically on a group of children with severe OI, who tend to experience the most fractures. To the authors' knowledge, this paper additionally presents the first anisotropic measures of bone material strength and macroscopic modulus of elasticity in "normal" pediatric bone.

Bone material properties were anisotropic in both groups (Table 3, longitudinal *vs*. transverse comparisons); however, anisotropy was less pronounced in the children with OI *vs*. controls. This reduced anisotropy in OI bone material properties may be a result of abnormalities at the ultra-structural level, such as reduced collagen content (Camacho et al., 1999), reduced spacing between collagen fibrils (Bart et al., 2014), and/or bone mineral crystals being smaller and less organized (Traub et al., 1994, Fratzl et al., 1996).

Compared to pediatric controls, modulus and strength measures in both directions were substantially lower in the OI group (Table 3). Although the differences in transverse modulus and yield strength between the groups were not found to be significant, it is possible that statistical significance may have been obtained with larger sample sizes. Interestingly, yield strain did not differ between the groups. These observations indicate that cortical bone in children with OI yields at a similar strain as normal bone, but this occurs under lower stress due to their lower modulus of elasticity.

Compared to controls, average vBMD was 22% lower and total porosity almost five times higher in the OI group (Table 4). These findings are consistent with other recent studies in which elevated intracortical porosity was observed in long bone shafts of children with OI (Jameson Jameson et al., 2013, Pazzaglia et al., 2013, Albert et al., 2014, Vardakastani et al., 2014). vTMD, however, did not differ significantly between the groups. This finding was surprising since abnormally elevated mineralization density has been observed in the iliac crests of children with OI (Boyde et al., 1999). It is possible that vTMD may have been lower at the surgical (diaphyseal) sites from which the specimens in the current study were obtained, where bowing was present and elevated bone modeling and remodeling activity was likely. However, in another recent study using a laboratory-based microcomputed tomography system with a polychromatic X-ray source, pediatric OI bone specimens obtained during similar procedures were reported to have slightly (10%) higher vTMD than controls (Imbert et al., 2014). The reason for these differing observations is not clear but may be attributed to differences in anatomic sites and testing methodologies. Nonetheless, the reduced vBMD observed in the long bone shafts of

children with severe OI appears to be a consequence of their elevated intracortical porosity rather than decreased vTMD.

Relationships have been established between bone material properties and density measures in human trabecular and cortical bone (Carter and Hayes, 1976, Keller, 1994, Keyak et al., 1994, Morgan et al., 2003). Current results confirmed that modulus of elasticity and strength decrease with decreases in vBMD in the long bone shafts of children with severe OI (Table 5). These relationships indicate that vBMD may be useful in estimating bone properties *in vivo* in the long bone shafts of children with OI. Further research is therefore warranted to determine whether volumetric bone mineral density measurements obtained at clinical scan resolutions (*e.g.*, by peripheral quantitative computed tomography) would enable appropriate estimation of cortical bone material properties in these children. In light of the increased intracortical porosity compared to controls (Table 4) and the negative (although not quite significant) relationship observed between bending strength and total porosity in the OI group (Table 5), it appears that a porous cortex contributes to long bone shaft fracture risk in children with severe OI. Increased intracortical porosity can reduce bone material strength substantially by decreasing the amount of bone material carrying the physiological loads and acting as stress risers (Currey, 1962, Yeni et al., 1997).

The bone material properties, on the other hand, were not related to vTMD. Thus, it appears that reduced bone material strength in children with severe OI is attributed primarily to the reduced quantity of bone tissue present within the cortical bone material rather than to inferior quality of the tissue. Nonetheless, the current study examined only two mineral parameters (*i.e.*, vBMD and vTMD). It is possible that other factors, such as microdamage (Hernandez et al., 2014), mineral size, shape, and arrangement (Cassella et al., 1995, Boskey, 2003), and/or collagen structure and crosslink density (Gautieri et al., 2009), also affect bone material strength in this population.

In normal pediatric bones, increases in modulus and strength occur between early childhood and adolescence (Currey and Butler, 1975). In the current study, however, bone material strength and modulus did not appear to increase with age in the children with severe OI. Nonetheless, due to limited sample size and other factors that could affect bone properties over time (*e.g.*, decreased physical activity (Takken et al., 2004, Sousa et al., 2014) and/or bisphosphonate treatments (Mashiba et al., 2000)), a definitive conclusion cannot be made at this time regarding relationships between cortical bone properties and age in children with severe OI.

Bisphosphonates are used commonly in the treatment of children with severe OI. These therapies have been associated with increased bone mass in the spine and reduced fracture occurrence in these children (Glorieux et al., 1998, Rauch et al., 2003, Bishop et al., 2010, Dwan et al., 2014). Their effect on cortical bone tissue quality in children with OI is not yet clear. Bisphosphonates can lead to decreased cortical bone material strength due to their impairment of cortical bone remodeling (Mashiba et al., 2000, Brock et al., 2015). However, abnormally elevated intracortical vascular porosity within the long bone shafts of children with OI (Pazzaglia et al., 2013, Albert et al., 2014) may enable new bone formation in cortical regions in spite of decreased osteoclastic activity. Thus, increases in cortical vBMD and bone material strength may be possible during this treatment. Nonetheless, further research is warranted to assess the effects of bisphosphonate therapies on cortical bone material properties in this patient population.

In conclusion, the main findings of this study are summarized as follows. In children with severe OI:

(1) Cortical bone material strength and modulus of elasticity are considerably lower than normal.

(2) Cortical bone exhibits anisotropic macroscopic material properties, but this anisotropy is less pronounced than in normal bone.

(3) Cortical bone yields at the same strain as do “normal” pediatric bones.

(4) Intracortical porosity is increased and vBMD is decreased, but vTMD is similar to that of pediatric controls.

(5) Cortical bone material strength and modulus of elasticity are correlated positively with vBMD but not with vTMD.

## Acknowledgements

The authors thank Kathy Reiners (Shriners Hospitals for Children – Chicago) for coordinating the OI bone specimen collection, and Dr. Cathy Carlson (University of Minnesota) for her help in procuring the normal pediatric control specimens. We are grateful for the assistance of beamline scientists Dr. Dula Parkinson and Dr. Alastair MacDowell (Advanced Light Source ALS, Lawrence Berkeley National Laboratory) in collecting the imaging data. We also thank Dr. Stephen M. Heinrich (Marquette University) for guidance on accounting for shear deformation in analyzing the mechanical data.

This work was supported by NIDRR grants H133P080005 and H133E100007 from the U.S. Department of Education, and grant UL1RR031973 from the Clinical and Translational Science Institute program of the National Center for Research Resources and the National Center for Advancing Translational Science. These contents, however, do not necessarily represent the policy of the Department of Education, and endorsement by the Federal Government should not be assumed. Finally, the study was also supported by research fellowships from Shriners Hospitals for Children as well as the ALS. The ALS is supported by the Director, Office of Science, Office of Basic Energy Sciences, of the U.S. Department of Energy under Contract No. DE-AC02-05CH11231.

## Conflict of interest

The authors have no conflicts of interest to disclose.

## Appendix A. Supplementary material

https://ars.els-cdn.com/content/image/1-s2.0-S0021929017304591-mmc1.docx

## References

Albert et al., 2013 C. Albert, J. Jameson, G. Harris
**Design and validation of bending test method for characterization of miniature pediatric cortical bone specimens**
Proc. Inst. Mech. Eng., Part H: J. Eng. Med., 227 (2) (2013), pp. 105-113

Albert et al., 2014 C. Albert, J. Jameson, P. Smith, G. Harris
**Reduced diaphyseal strength associated with high intracortical vascular porosity within long bones of children with osteogenesis imperfecta**
Bone, 66 (2014), pp. 121-130

ASTM-D790-07, 2006 ASTM-D790-07

**Standard Methods for Flexural Properties of Unreinforced and Reinforced Plastics and Electrical Insulating Materials**
ASTM International, West Conshohocken, PA, USA (2006)

Bart et al., 2014 Z.R. Bart, M.A. Hammond, J.M. Wallace
**Multi-scale analysis of bone chemistry, morphology and mechanics in the oim model of osteogenesis imperfecta**
Connect. Tissue Res., 55 (Suppl. 1) (2014), pp. 4-8

Bishop et al., 2010 N. Bishop, R. Harrison, F. Ahmed, N. Shaw, R. Eastell, M. Campbell, E. Knowles, C. Hill, C. Hall, S. Chapman, A. Sprigg, A. Rigby
**A randomized, controlled dose-ranging study of risedronate in children with moderate and severe osteogenesis imperfecta**
J. Bone Miner. Res., 25 (1) (2010), pp. 32-40

Boskey, 2003 A.L. Boskey
**Bone mineral crystal size**
Osteoporos. Int., 14 (Suppl. 5) (2003), pp. S16-S21

Boyde et al., 1999 A. Boyde, R. Travers, F.H. Glorieux, S.J. Jones
**The mineralization density of iliac crest bone from children with osteogenesis imperfecta**
Calcif. Tissue Int., 64 (3) (1999), pp. 185-190

Brock et al., 2015 G.R. Brock, J.T. Chen, A.R. Ingraffea, J. MacLeay, G.E. Pluhar, A.L. Boskey, M.C. van der Meulen
**The effect of osteoporosis treatments on fatigue properties of cortical bone tissue**
Bone Rep, 2 (2015), pp. 8-13

Byers and Steiner, 1992 P.H. Byers, R.D. Steiner
**Osteogenesis imperfecta**
Annu. Rev. Med., 43 (1992), pp. 269-282

Camacho et al., 1999 N.P. Camacho, L. Hou, T.R. Toledano, W.A. Ilg, C.F. Brayton, C.L. Raggio, L. Root, A.L. Boskey
**The material basis for reduced mechanical properties in oim mice bones**
J. Bone Miner. Res., 14 (2) (1999), pp. 264-272

Caouette et al., 2016 C. Caouette, N. Ikin, I. Villemure, P.J. Arnoux, F. Rauch, C.E. Aubin
**Geometry reconstruction method for patient-specific finite element models for the assessment of tibia fracture risk in osteogenesis imperfecta**
Med. Biol. Eng. Comput., 55 (4) (2016), pp. 549-560

Caouette et al., 2014 C. Caouette, F. Rauch, I. Villemure, P.J. Arnoux, M. Gdalevitch, L.N. Veilleux, J.L. Heng, C.E. Aubin
**Biomechanical analysis of fracture risk associated with tibia deformity in children with osteogenesis imperfecta: a finite element analysis**
J. Musculoskelet Neuronal Interact, 14 (2) (2014), pp. 205-212

Cardoso et al., 2013 L. Cardoso, S.P. Fritton, G. Gailani, M. Benalla, S.C. Cowin
**Advances in assessment of bone porosity, permeability and interstitial fluid flow**
J. Biomech., 46 (2) (2013), pp. 253-265

Carter and Hayes, 1976 D.R. Carter, W.C. Hayes
**Bone compressive strength: the influence of density and strain rate**
Science, 194 (4270) (1976), pp. 1174-1176

Carter et al., 2013 Y. Carter, C.D. Thomas, J.G. Clement, A.G. Peele, K. Hannah, D.M. Cooper
**Variation in osteocyte lacunar morphology and density in the human femur–a synchrotron radiation micro-CT study**
Bone, 52 (1) (2013), pp. 126-132

Cassella et al., 1995 J.P. Cassella, N. Garrington, T.C. Stamp, S.Y. Ali
**An electron probe X-ray microanalytical study of bone mineral in osteogenesis imperfecta**
Calcif. Tissue Int., 56 (2) (1995), pp. 118-122
Choi et al., 1990 K. Choi, J.L. Kuhn, M.J. Ciarelli, S.A. Goldstein
**The elastic moduli of human subchondral, trabecular, and cortical bone tissue and the size-dependency of cortical bone modulus**
J. Biomech., 23 (11) (1990), pp. 1103-1113
Cooper et al., 2003 D.M. Cooper, A.L. Turinsky, C.W. Sensen, B. Hallgrimsson
**Quantitative 3D analysis of the canal network in cortical bone by micro-computed tomography**
Anat. Rec. B New Anat., 274 (1) (2003), pp. 169-179
Currey, 1962 J. Currey
**Stress concentrations in bone**
Q. J. Microsc. Sci., 103 (1) (1962), pp. 111-133
Currey and Pond, 1989 J. Currey, C. Pond
**Mechanical properties of very young bone in the axis deer (Axis axis) and humans**
J. Zool., 218 (1989), pp. 59-87
Currey and Butler, 1975 J.D. Currey, G. Butler
**The mechanical properties of bone tissue in children**
J. Bone Joint Surg. Am., 57 (6) (1975), pp. 810-814
Dong et al., 2014 P. Dong, S. Haupert, B. Hesse, M. Langer, P.J. Gouttenoire, V. Bousson, F. Peyrin
**3D osteocyte lacunar morphometric properties and distributions in human femoral cortical bone using synchrotron radiation micro-CT images**
Bone, 60 (2014), pp. 172-185
Doube et al., 2010 M. Doube, M. Klosowski, I. Arganda-Carreras, F. Cordelieres, R. Dougherty, J. Jackson, B. Schmid, J. Hutchinson, S. Schefelbine
**BoneJ: free and extensible bone image analysis in ImageJ**
Bone, 47 (6) (2010), pp. 1076-1079
Dwan et al., 2014 K. Dwan, C.A. Phillipi, R.D. Steiner, D. Basel
**Bisphosphonate therapy for osteogenesis imperfecta**
Cochrane Database Syst. Rev. (7) (2014)
CD005088
Fratzl et al., 1996 P. Fratzl, O. Paris, K. Klaushofer, W.J. Landis
**Bone mineralization in an osteogenesis imperfecta mouse model studied by small-angle X-ray scattering**
J. Clin. Invest., 97 (2) (1996), pp. 396-402
Fritz et al., 2009a J.M. Fritz, Y. Guan, M. Wang, P.A. Smith, G.F. Harris
**A fracture risk assessment model of the femur in children with osteogenesis imperfecta (OI) during gait**
Med. Eng. Phys., 31 (9) (2009), pp. 1043-1048
Fritz et al., 2009b J.M. Fritz, Y. Guan, M. Wang, P.A. Smith, G.F. Harris
**Muscle force sensitivity of a finite element fracture risk assessment model in osteogenesis imperfecta - Biomed 2009**
Biomed. Sci. Instrum., 45 (2009), pp. 316-321
Gautieri et al., 2009 A. Gautieri, S. Uzel, S. Vesentini, A. Redaelli, M.J. Buehler
**Molecular and mesoscale mechanisms of osteogenesis imperfecta disease in collagen fibrils**
Biophys. J., 97 (3) (2009), pp. 857-865
Glorieux et al., 1998 F.H. Glorieux, N.J. Bishop, H. Plotkin, G. Chabot, G. Lanoue, R. Travers

**Cyclic administration of pamidronate in children with severe osteogenesis imperfecta**
N. Engl. J. Med., 339 (14) (1998), pp. 947-952

Hernandez et al., 2014
C.J. Hernandez, F.M. Lambers, J. Widjaja, C. Chapa, C.M. Rimnac**Quantitative relationships between microdamage and cancellous bone strength and stiffness**
Bone, 66 (2014), pp. 205-213
ArticleDownload PDFView Record in Scopus

Hirsch and Evans, 1965 C. Hirsch, F.G. Evans
**Studies on some physical properties of infant compact bone**
Acta Orthopaedica Scandinavica, 35 (1965), pp. 300-303

Hubbell, 1982 J.H. Hubbell
**Photon mass attenuation and energy-absorption coefficients from 1 keV to 20 MeV**
Int. J. Appl. Radiat. Isot., 33 (1982), pp. 1269-1290

Imbert et al., 2014 L. Imbert, J.C. Auregan, K. Pernelle, T. Hoc
**Mechanical and mineral properties of osteogenesis imperfecta human bones at the tissue level**
Bone, 65 (2014), pp. 18-24

Imbert et al., 2015 L. Imbert, J.C. Auregan, K. Pernelle, T. Hoc
**Microstructure and compressive mechanical properties of cortical bone in children with osteogenesis imperfecta treated with bisphosphonates compared with healthy children**
J. Mech. Behav. Biomed. Mater., 46 (2015), pp. 261-270

Jameson et al., 2013 Jameson, J., Albert, C., Busse, B., Smith, P., Harris, G., 2013. 3D micron-scale imaging of the cortical bone canal network in human osteogenesis imperfecta (OI). In: Weaver, J.B., Molthen, R.C. (Eds.), Proceedings of SPIE, Medical Imaging 2013: Biomedical Applications in Molecular, Structural, and Functional Imaging. International Society for Optics and Photonics, Lake Buena Vista, FL.

Keller, 1994 T.S. Keller
**Predicting the compressive mechanical behavior of bone**
J. Biomech., 27 (9) (1994), pp. 1159-1168

Keyak et al., 1994 J.H. Keyak, I.Y. Lee, H.B. Skiner
**Correlations between orthogonal mechanical properties and density of trabecular bone: use of different densitometric measures**
J. Biomed. Mater. Res., 28 (1994), pp. 1329-1336

MacDowell et al., 2012 MacDowell, A.A., Parkinson, D.Y., Haboub, A., Schaible, E., Nasiatka, J.R., Yee, C.A., Jameson, J.R., Ajo-Franklin, J.B., Brodersen, C.R., McElrone, A.J., 2012. X-ray micro-tomography at the Advanced Light Source. In: SPIE 8506: Developments in X-ray Tomography VIII. International Society for Optics and Photonics, San Diego, CA.

Marini, 2011 Marini, J.C., 2011. Chapter 692 Osteogenesis imperfecta. In: Kliegman, R.M., Stanton, B.F., Schor, N.F., St. Geme, J.W., Behrman, R.E. (Eds.), Nelson Textbook of Pediatrics. Elsevier, Philadelphia, PA.

Mashiba et al., 2000 T. Mashiba, T. Hirano, C.H. Turner, M.R. Forwood, C.C. Johnston, D.B. Burr
**Suppressed bone turnover by bisphosphonates increases microdamage accumulation and reduces some biomechanical properties in dog rib**
J. Bone Miner. Res., 15 (4) (2000), pp. 613-620

McCreadie et al., 2004 B.R. McCreadie, S.J. Hollister, M.B. Schaffler, S.A. Goldstein
**Osteocyte lacuna size and shape in women with and without osteoporotic fracture**
J. Biomech., 37 (4) (2004), pp. 563-572

Morgan et al., 2003 E.F. Morgan, H.H. Bayraktar, T.M. Keaveny

**Trabecular bone modulus-density relationships depend on anatomic site**
J. Biomech., 36 (7) (2003), pp. 897-904

Ohman et al., 2011 C. Ohman, M. Baleani, C. Pani, F. Taddei, M. Alberghini, M. Viceconti, M. Manfrini
**Compressive behaviour of child and adult cortical bone**
Bone (2011)

Parfitt et al., 1987 A.M. Parfitt, M.K. Drezner, F.H. Glorieux, J.A. Kanis, H. Malluche, P.J. Meunier, S.M. Ott, R.R. Recker
**Bone histomorphometry: standardization of nomenclature, symbols, and units. Report of the ASBMR Histomorphometry Nomenclature Committee**
J. Bone Miner. Res., 2 (6) (1987), pp. 595-610

Pazzaglia et al., 2013 U.E. Pazzaglia, T. Congiu, P.C. Brunelli, L. Magnano, A. Benetti
**The long bone deformity of osteogenesis imperfecta III: analysis of structural changes carried out with scanning electron microscopic morphometry**
Calcif. Tissue Int., 93 (5) (2013), pp. 453-461

Rauch et al., 2003 F. Rauch, H. Plotkin, L. Zeitlin, F.H. Glorieux
**Bone mass, size, and density in children and adolescents with osteogenesis imperfecta: effect of intravenous pamidronate therapy**
J. Bone Miner. Res., 18 (4) (2003), pp. 610-614

Ridler and Calvard, 1978 T.W. Ridler, S. Calvard
**Picture thresholding using an interative selection method**
IEEE Trans. Syst. Man Cybernetics, 8 (1978), pp. 630-632

Schneider et al., 2012 C.A. Schneider, W.S. Rasband, K.W. Eliceiri
**NIH Image to ImageJ: 25 years of image analysis**
Nat. Methods, 9 (7) (2012), pp. 671-675

Sillence et al., 1979 D.O. Sillence, A. Senn, D.M. Danks
**Genetic heterogeneity in osteogenesis imperfecta**
J. Med. Genet., 16 (2) (1979), pp. 101-116

Sousa et al., 2014 T. Sousa, V. Bompadre, K.K. White
**Musculoskeletal functional outcomes in children with osteogenesis imperfecta: associations with disease severity and pamidronate therapy**
J. Pediatr. Orthop., 34 (1) (2014), pp. 118-122

Takken et al., 2004 T. Takken, H.C. Terlingen, P.J. Helders, H. Pruijs, C.K. Van der Ent, R.H. Engelbert
**Cardiopulmonary fitness and muscle strength in patients with osteogenesis imperfecta type I**
J. Pediatr., 145 (6) (2004), pp. 813-818

Traub et al., 1994 W. Traub, T. Arad, U. Vetter, S. Weiner
**Ultrastructural studies of bones from patients with osteogenesis imperfecta**
Matrix Biol., 14 (4) (1994), pp. 337-345

Vardakastani et al., 2014 V. Vardakastani, D. Saletti, W. Skalli, P. Marry, J.M. Allain, C. Adam
**Increased intra-cortical porosity reduces bone stiffness and strength in pediatric patients with osteogenesis imperfecta**
Bone, 69 (2014), pp. 61-67

Wallace et al., 2014 R. Wallace, P. Pankaj, A. Simpson
**Major source of error when calculating bone mechanical properties**
J. Bone Miner. Res., 29 (12) (2014), p. 2697

Yeni et al., 1997 Y.N. Yeni, C.U. Brown, Z. Wang, T.L. Norman
**The influence of bone morphology on fracture toughness of the human femur and tibia**
Bone, 21 (5) (1997), pp. 453-459